



**Granular packings with sliding, rolling, and twisting friction**A. P. Santos <sup>\*</sup>, Dan S. Bolintineanu, Gary S. Grest, Jeremy B. Lechman, Steven J. Plimpton, and Ishan Srivastava <sup>†</sup>  
*Sandia National Laboratories, Albuquerque, New Mexico 87185, USA*Leonardo E. Silbert *School of Math, Science and Engineering, Central New Mexico Community College, Albuquerque, New Mexico 87106, USA*

(Received 22 July 2020; accepted 21 August 2020; published 16 September 2020)

Intuition tells us that a rolling or spinning sphere will eventually stop due to the presence of friction and other dissipative interactions. The resistance to rolling and spinning or twisting torque that stops a sphere also changes the microstructure of a granular packing of frictional spheres by increasing the number of constraints on the degrees of freedom of motion. We perform discrete element modeling simulations to construct sphere packings implementing a range of frictional constraints under a pressure-controlled protocol. Mechanically stable packings are achievable at volume fractions and average coordination numbers as low as 0.53 and 2.5, respectively, when the particles experience high resistance to sliding, rolling, and twisting. Only when the particle model includes rolling and twisting friction were experimental volume fractions reproduced.

DOI: [10.1103/PhysRevE.102.032903](https://doi.org/10.1103/PhysRevE.102.032903)**I. INTRODUCTION**

A rolling or spinning marble on a table eventually slows to a stop because of resistance to the rolling and twisting modes of motion. However, rolling and twisting friction are often excluded in simulation studies because of the added complexity of the contact mechanics model. Such approximations may be valid for some phenomena and materials, such as materials with low sliding friction [1], but the validity of this approximation, and the ability to match experimental properties, must be tested.

Simulations have found that rolling and twisting friction is necessary to reproduce experimental observations and can change macroscopic behavior. Only by including rolling friction were Mort *et al.* [2] able to reproduce experimental shear-to-normal stress ratio in a hopper. Singh *et al.* [3] were also unable to reproduce experimental shear viscosity at relevant sliding friction coefficients with simulations without rolling friction. Other simulations found that rolling friction induces columnar granular particle contact backbones [4], increases stress-dilatancy behavior [5], causes anisotropic dense granular flows [6], and provides an explanation of discontinuous shear thickening [7,8]. Simulations of shear banding [9,10], rigid flat punch [11], and wing-crack extension [12] processes generated large regions of rotations. Resistance to such rotation could change behavior, and studies of such processes should consider including rolling and twisting friction in models. The magnitude of resistance to rolling and twisting

can be approximated, and explained by, contact mechanics theory.

Long before granular particles were simulated with rolling and twisting friction, Reynolds [13] and Hertz [14] used theories of rolling and twisting resistance to suggest a substantial impact on packing structure. These theories focus on single particle-wall interactions using elastic and inelastic approximations of rolling resistance [15,16]. Twisting and sliding friction have the same origins—twisting having rotational instead of translational displacements over the contact area. Rolling friction originates from a combination of microslip at the interface, inelastic deformation, and surface roughness that create a pressure difference between the leading and trailing ends of the rolling contact [17]. Constraint counting predicts that rolling and twisting resistance leads to large changes in packing structure (see Sec. III A). Particle properties, including surface morphology and the material [17], sets the rolling and twisting resistance and thus can control packing structure.

Packings of spheres and disks with sliding friction have shown many interesting phenomena. For example, in three dimensions, the coordination number  $Z$  decreases gradually with friction from the frictionless value of  $Z = 6$  to the frictional isostatic number  $Z = 4$  [18–22]. The volume fraction  $\phi$  follows the decrease in coordination number with increasing friction. Frictionless hard spheres sets the densest volume fraction  $\phi \sim 0.64$  for random packings, known as the maximally random jammed state [23]. Simulations [18] and theory [21] have shown that sliding friction leads to looser granular sphere packings than frictionless sphere packings, as verified by experiments [24].

How loose frictional packings can be depends on the friction coefficient and the path to packing. Early packing experiments of monodisperse spheres measured a range of volume fractions with minimums of  $\phi \sim 0.57$ –0.6 [25–27].

<sup>\*</sup>asanto@sandia.gov<sup>†</sup>Present address: Center for Computational Sciences and Engineering, Lawrence Berkeley National Laboratory, Berkeley, California 94720, USA

Later experiments demonstrated that materials with larger friction coefficients can access mechanically stable packings with lower volume fractions [24,28,29]. With careful, density-matched experiments, Farrell *et al.* [29] measured volume fractions  $\phi < 0.54$  for very frictional particles. Silbert [22] used a volume-controlled simulation protocol to produce stable packings as low as  $\phi = 0.576$  for high, but realistic sliding friction coefficient values ( $\mu_s = 0.5$ ), which is still above the experimental value. Because rolling and twisting friction makes models more realistic, it offers simulations a route to match the low volume fractions seen in experimental packings of frictional particles.

Packings generated with a volume-controlled protocol have difficulty forming stable packings at low pressures and volume fractions. By controlling pressure not volume, final packings repeatably and rigorously satisfy set stress conditions at low pressures. Pressure-controlled protocols have been used to study granular packings [19,30–32], but their application to three-dimensional (3D) frictional particles is less common. In this article, a constant pressure in the  $x$ ,  $y$ , and  $z$  directions allows the box to adjust the edge length, and by allowing the box to adopt triclinic configurations, constant zero shear stresses are achieved. Packings formed by pressure-controlled protocols are more stable to shear deformation than volume-controlled methods, as shown by Dagois-Bohy *et al.* [30] and Smith *et al.* [31].

In this article, a constant-pressure protocol is used to pack 3D, monodisperse particles with varying degrees of sliding, rolling, and twisting friction. The equations of motion that define contact forces for the normal, sliding, rolling, and twisting modes are presented in Sec. II A. The appropriate magnitudes of the rolling and twisting contact force parameters are discussed in the Appendix. The details and benefits of the constant-pressure packing protocol are described in Sec. II B. The effect of rolling and twisting friction on packing morphology is first predicted using constraint counting (Sec. III A), and then the results of numerical simulations are presented and compared to experiment in Sec. III B.

## II. METHODOLOGY

### A. Contact model

Granular particles are modeled as spherical particles with radius  $R_i$  and mass  $m_i$ . Particles interact only when in contact, through a spring-dashpot-slider interaction potential for the normal, sliding, rolling, and twisting modes of motion. Sliding friction uses the Cundall and Strack model [33]. Rolling resistance is based on Luding's implementation [34], and twisting resistance is based on Marshall's implementation [35]. For two granular particles in contact, separated by a distance  $|\mathbf{r}_{ij}| < R_i + R_j$ , the force on particle  $i$  from particle  $j$  is

$$\mathbf{F}_{ij} = \mathbf{F}_n + \mathbf{F}_s, \quad (1a)$$

$$\mathbf{F}_n = k_n \delta \mathbf{n} - m_{\text{eff}} \gamma_n \mathbf{v}_n, \quad (1b)$$

$$\mathbf{F}_s = -\min(\mu_s |\mathbf{F}_n|, |-k_s \xi_s - m_{\text{eff}} \gamma_s \mathbf{v}_s|) \frac{\mathbf{v}_s}{|\mathbf{v}_s|}, \quad (1c)$$

where  $\delta = R_i + R_j - |\mathbf{r}_{ij}|$ ,  $\mathbf{n} = \frac{\mathbf{r}_{ij}}{|\mathbf{r}_{ij}|}$ ,  $m_{\text{eff}} = \frac{m_i m_j}{m_i + m_j}$ .  $\mathbf{F}_n$  is the normal force, and  $\mathbf{F}_s$  is the sliding force. Sliding ( $s$ ), rolling

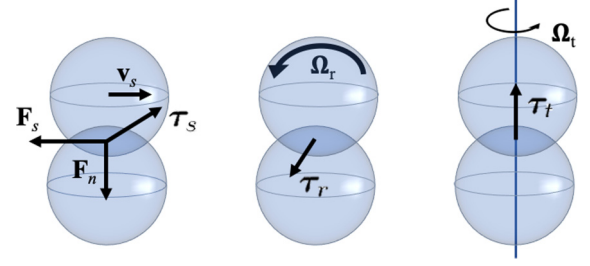


FIG. 1. Schematic of the granular particle interaction model normal  $\mathbf{F}_n$  and sliding  $\mathbf{F}_s$  forces, and the sliding  $\tau_s$ , rolling  $\tau_r$ , and twisting  $\tau_t$  torques. Resistance to the sliding translational velocity  $\mathbf{v}_s$ , the rolling  $\Omega_r$ , and twisting  $\Omega_t$  rotational velocities causes frictional forces and torques.

( $r$ ), and twisting ( $t$ ) give rise to torque when granular particles are in contact. The torque acting on particle  $i$  due to contact with particle  $j$  is defined as

$$\boldsymbol{\tau}_{ij} = \boldsymbol{\tau}_s + \boldsymbol{\tau}_r + \boldsymbol{\tau}_t, \quad (2a)$$

$$\boldsymbol{\tau}_s = -\left(R_i - \frac{\delta}{2}\right) \mathbf{n} \times \mathbf{F}_s, \quad (2b)$$

$$\boldsymbol{\tau}_r = -R_{\text{eff}} \mathbf{n} \times \min(\mu_r |\mathbf{F}_n|, |-k_r \xi_r - \gamma_r \mathbf{v}_r|) \frac{\mathbf{v}_r}{|\mathbf{v}_r|}, \quad (2c)$$

$$\boldsymbol{\tau}_t = -\min(\mu_t |\mathbf{F}_n|, -k_t \xi_t - \gamma_t v_t) \mathbf{n}, \quad (2d)$$

where  $R_{\text{eff}} = \frac{R_i R_j}{R_i + R_j}$ . Note that torque acting on particle  $j$  due to contact with particle  $i$  is  $\boldsymbol{\tau}_{ji} = -\boldsymbol{\tau}_{ij}$ , except for  $\boldsymbol{\tau}_s$  if  $R_i \neq R_j$ . Each mode of motion  $m$  has a Hookean spring constant  $k_m$  and viscoelastic damping coefficient  $\gamma_m$  that takes into account the inelasticity of the contact mechanics. The Coulomb yield criteria is applied to each frictional mode force or torque and sets the maximum to be the friction coefficient  $\mu_m$  times the normal force.

The displacement accumulated as particles are in contact is an important aspect of this model because it captures microslip and has been observed in experimental studies of oblique impact [36]. The accumulated displacement is measured by  $\boldsymbol{\xi}_m = \int_{t_0}^t \mathbf{v}_m(\tau) d\tau$ , where  $t_0$  is the time at first contact. To compensate for the effect of rigid body rotations,  $\boldsymbol{\xi}_m$  is calculated in the reference frame of the rotating particle pair [34]. As the contacting pair rotates as a rigid body, the tangential and rolling displacement vector components that are parallel to  $\mathbf{n}$  are subtracted at each time step and scaled to preserve their magnitude. The velocity of each of the four modes  $\mathbf{v}_m$  is relative to the contact vector, and these are defined as

$$\mathbf{v}_n = [(\mathbf{v}_j - \mathbf{v}_i) \cdot \mathbf{n}] \mathbf{n}, \quad (3a)$$

$$\mathbf{v}_s = (\mathbf{v}_j - \mathbf{v}_i) - [(\mathbf{v}_j - \mathbf{v}_i) \cdot \mathbf{n}] \mathbf{n} - (R_i \boldsymbol{\Omega}_i + R_j \boldsymbol{\Omega}_j) \times \mathbf{n}, \quad (3b)$$

$$\mathbf{v}_r = -R_{\text{eff}} (\boldsymbol{\Omega}_i - \boldsymbol{\Omega}_j) \times \mathbf{n}, \quad (3c)$$

$$v_t = (\boldsymbol{\Omega}_i - \boldsymbol{\Omega}_j) \cdot \mathbf{n}, \quad (3d)$$

where  $\mathbf{v}_i$  and  $\boldsymbol{\Omega}_i$  are the translational and rotational velocities, respectively. The twisting velocity is a scalar because it is one component of the rotational degrees of freedom. Figure 1

visualizes the three modes of friction and the associated velocities, forces, and torques.

The assumption of linear elastic behavior for interparticle contacts is reasonably accurate as a model for sufficiently stiff particles. Note that as an upper limit, for example, glass has a yield stress  $\sigma_y \approx 70$  MPa and would be expected to yield, fracture, or fragment, deviating significantly from spherical shape, for  $P_a \gg 10^{-3} \frac{k_n}{d}$ . Most simulations were run at  $P_a = 10^{-4} \frac{k_n}{d}$  where  $d$  is the diameter.

In all simulations, particles have the same radius  $R_i = R = 0.5$  and mass  $m_i = m = 1$ . The particle spring and damping parameters are set equal to each other,  $k_n = k_s = k_r = k_t = 1.0 m/\tau^2$  and  $\gamma_n = \gamma_s = \gamma_r = \gamma_t = 0.5 \tau^{-1}$ , where  $m$  is the particle mass and  $\tau = \sqrt{m/k_n}$  [37]. The model parameters and coefficients of rolling and twisting friction used in this study are not based on a specific material. However, the chosen parameters are within relevant values, determined by simulations and a contact mechanics analysis. The contact mechanics analysis and details of two-overlapping-spheres simulations are in the Appendix. Changes within an order of magnitude of  $k_m$  and  $\gamma_m$  did not yield qualitative changes in the packing behavior. If  $k_r$  or  $k_t$  are orders of magnitude lower than  $k_n$  and the normal force is small, the torque resistances are negligible. The key parameters varied in the analysis presented here of packings are the coefficients of the different friction modes, not the spring and damping coefficients. A wide range of friction coefficients are studied that include and go above values for typical materials. For example, copper, bronze, and steel spheres have coefficients of rolling resistance  $\mu_r$  of  $10^{-4}$  to  $10^{-2}$  [38,39], while viscoelastic materials have values of  $10^{-3}$  to  $10^{-2}$  [40]. In this study,  $\mu_{r,t}$  varies from 0 to 100 because of precedent set by previous simulation studies [2,19,22] and to understand the range of impact of rolling twisting friction for this model.

### B. Constant pressure packing simulations

The contact model described in Sec. II A was used to perform discrete element, particle-based simulations in LAMMPS [41] by integrating Newton's second law with the velocity-Verlet integration scheme. The particle positions and orientations are updated based on the interparticle forces  $\mathbf{F}_i$  and torques  $\boldsymbol{\tau}_i$  calculated by Eqs. (1a) and (2a). The equations of motion include the degrees of freedom for a deforming box to simulate granular particles under a constant applied pressure tensor. The granular particles are placed within a fully periodic 3D box which is able to change shape with triclinic deformations to maintain the applied pressure tensor. A barostat was used in the  $N\mathbf{P}_aH$  ensemble to integrate the positions and momenta of the particles and box, where  $N$  is the number of particles,  $\mathbf{P}_a$  is the applied pressure tensor, and  $H$  is the enthalpy. The Shinoda-Shiga-Mikami [42] formulation used in this study combines the hydrostatic equations of Martyna *et al.* [43] with the strain energy proposed by Parrinello and Rahman [44].

For each friction state measured, six packings of  $N = 10^4$  diameter  $d = 1$  nonoverlapping particles were generated. Simulations were initialized with particles at random positions and low volume fraction  $\phi_0 = 0.05$ . The initial volume fraction  $\phi_0$  does not affect the properties of the final packing

TABLE I. The average number of contacts per particle  $Z$  needed to satisfy the number of constraints per contact  $N^c$  for a mechanically stable packing due to sliding, rolling, twisting, and the various friction combinations for 3D and 2D particles. The inclusion “y” or exclusion “n” of a friction mode determines  $N^c$ . Two-dimensional particles do not have the twisting mode and values are omitted accordingly.

	Friction			3D		2D	
	Sliding	Rolling	Twisting	$N^c$	$Z$	$N^c$	$Z$
n	n	n	n	1	6	1	4
y	n	n	n	3	4	2	3
n	y	n	n	3	4	2	3
n	n	y	y	2	6	–	–
y	y	n	n	5	12/5	3	2
y	n	y	y	4	3	–	–
n	y	y	y	4	3	–	–
y	y	y	y	6	2	–	–

studied here, so long as  $\phi_0$  is not too near, or above, the final volume fraction ( $\phi_0 < \phi - 0.3$ ). Initial particle translational and rotational velocities were set to zero. The simulation time step was set to  $\delta t = 0.02\tau$ . A time step of  $0.002\tau$  did not change the results for the systems studied within the uncertainties.

After initialization, the particles are isotropically compressed. The packing method begins with a system at  $\phi_0 = 0.05$  and  $P = 0$ , then at  $t = 0$  a constant pressure  $P_a$  with a pressure damping of  $P_{\text{damp}} = 2.25 \tau^{-1}$  is applied until the system jams. The applied pressure has been shown to affect the final volume fraction and coordination number with or without friction of any mode, as observed previously [19,22,45–47]. Most of the simulations presented here are for  $P_a = 10^{-4} \frac{k_n}{d}$ , which, as we show below, is in the low-pressure regime. Simulations were run until the per-particle kinetic energy  $U^{\text{kinetic}}/N < 10^{-12} k_n d$ , which was well after the volume fraction to stops developing. For  $P_a = 10^{-4} \frac{k_n}{d}$ , the total run time was  $t/\tau = 2 \times 10^5$ , and for  $P_a = 10^{-7} \frac{k_n}{d}$ , the total run time was  $t/\tau = 4 \times 10^6$ . The applied symmetric pressure tensor  $\mathbf{P}_a$  is defined as  $P_a = P_{a,xx} = P_{a,yy} = P_{a,zz}$  and  $P_{a,xy} = P_{a,xz} = P_{a,yz} = 0$  [48]. The applied and measured pressure tensors equal each other exactly,  $\mathbf{P}_{\text{int}} = \mathbf{P}_a$ , in the final packings. Because the shear pressures are so near zero, these packings are stable to small deformations.

The volume fraction  $\phi$  and coordination number  $Z$  are the key parameters measured in this study. These properties were averaged over the six packings generated from the final simulation configurations. Measured values of  $Z$  are calculated without “rattlers,” particles that have too few contacts to contribute to the mechanical stability of the packings. Particles were classified as rattlers if  $Z_i \leq N_{\text{ratt}}^c$ , where  $Z_i$  is the number of contacts of particle  $i$  and  $N_{\text{ratt}}^c$  is a friction-dependent minimum number of constraints on the degrees of freedom of motion. Each mode of friction contributes constraints to  $N_{\text{ratt}}^c$ . The friction contributions are determined with constraint counting (see Sec. III A), and the values of  $N_{\text{ratt}}^c = N^c/2$ , where  $N^c$  is the value in Table I. An intermediate friction of  $\mu_m^c = 0.01$  was used to determine whether the sliding, rolling, and/or twisting friction mode  $m$  would contribute to  $N_{\text{ratt}}^c$ .

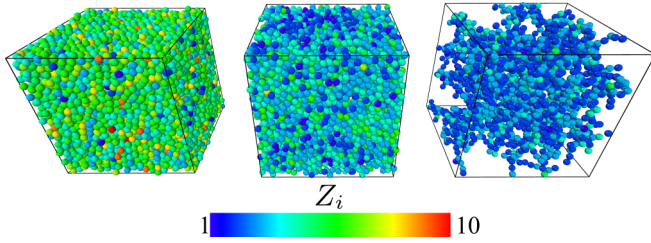


FIG. 2. Configurations of mechanically stable granular particle packings at three different sliding  $s$ , rolling  $r$ , and twisting  $t$  friction states: low ( $\mu_s = \mu_r = \mu_t = 0$ , left), intermediate ( $\mu_s = \mu_r = \mu_t = 0.3$ , middle), and high ( $\mu_s = \mu_r = \mu_t = 1$ , right). Rattlers have been removed from the visualization, and each granular particle is colored based on the number of local contacts  $Z_i$ .

which determines the row in Table I. The value of  $\mu_m^c = 0.01$  was chosen because it is the point where friction has an appreciable impact on  $\phi$  and  $Z$ . Other choices of  $\mu_m^c$  did not lead to large changes in  $Z$ . Rattlers are identified iteratively, so that the number of contacts per particle decreases based on the number of rattlers in contact with the particle. If the number of contacts decreases enough to constitute a rattler, by removing neighboring rattlers, it is counted as such.

### III. RESULTS

Representative packed granular particle configurations which demonstrate that the inclusion of sliding, rolling, and twisting friction causes major microstructural change are shown in Fig. 2. Though each system has 10 000 particles, the volume of each is slightly different. Rattlers, which are particles that do not have enough contacts to be mechanically stable because they can move within a mechanically stable packed system, are not visualized (see Sec. II B for rattler identification details). The fraction of rattlers increases with the friction coefficient and the number of friction modes. As the sliding, rolling, and twisting friction coefficients increase, particles are more likely to have fewer contacts; see the color change of particles in Fig. 2. The structure and small fraction of nonrattlers at high sliding  $\mu_s$ , rolling  $\mu_r$ , and twisting  $\mu_t$  frictions differ considerably from the case where  $\mu_s = \mu_r = \mu_t = 0$  or even  $\mu_s = \mu_r = \mu_t = 0.3$ . The drastic decrease in the average number of contacts per particle with multiple friction modes can be predicted by balancing contact forces and constraints for a mechanically stable packing.

#### A. Constraint counting

Constraint counting models a packing as a state where the total number of forces and torques on the granular particles equals the total number of constraining contacts to satisfy Maxwell's rigidity criterion [49]. For  $N$  granular particles in  $d$  dimensions there are  $N$  normal forces and, if there is friction,  $(d-1)N$  tangential forces,  $N$  torques for  $d=2$ , and  $3N$  torques for  $d=3$ . For mechanical stability, these forces and torques must be balanced by the total *constraining* contacts  $NZ$ , where  $Z$  is the average number of contacts per particle. The analysis here assumes that any contact, no matter how close it is to the friction limit, is constraining. Each constraint

mode  $m$  contributes to the number of constraints per contact,  $N^c = \sum_m N_m^c$ . The normal contact force law of a hard sphere contributes  $N_n^c = 1$ , although for real or simulated hard granular particles, without adhesion, it is constrained only in the repulsive direction. The number of constraints per contact for the other modes in three dimensions are  $N_s^c = 2$ ,  $N_r^c = 2$ , and  $N_t^c = 1$ . In two dimensions,  $N_s^c = 1$ ,  $N_r^c = 1$ , and  $N_t^c = 0$ . The total number of constraints and equations  $N^{\text{eqn}}$  are then set to equal each other, so that

$$N^{\text{eqn}} = \begin{cases} 6N, & 3\text{D, frictional} \\ 3N, & 2\text{D, frictional} \\ 3N, & 3\text{D, frictionless} \\ 2N, & 2\text{D, frictionless} \end{cases}, \quad (4a)$$

$$N^{\text{eqn}} = \frac{N^c}{2} N \langle Z \rangle, \quad (4b)$$

$$\langle Z \rangle = \frac{2N^{\text{eqn}}}{N^c N}, \quad (4c)$$

since a packing has to balance  $dN$  forces and  $3N$  (3D) or  $1N$  [two-dimensional (2D)] torques for frictional particles. The number of local constraints  $N_c^{\text{local}}$ , which are used to identify rattlers in the simulation configuration analysis, is  $N_c^{\text{local}} = N_c/2$ . Table I lists the  $N_c$  and  $Z$  calculated from constraint counting using Eq. (4c). The low value of  $Z = 2$  when all modes of friction are constraining was previously calculated by Liu *et al.* [50]. The predictions for  $Z$  with different modes are compared to simulation results in Sec. III B.

#### B. Packing structure with rolling and twisting

Even though constraint counting predicts that rolling and twisting resistances cause large changes in  $Z$ , simulations often ignore resistance to rolling and twisting. Simulations of many particles with the isotropic compression method described in Sec. II B can test the constraint counting predictions and compare with experimental measurements of mechanically stable packing. Mechanically stable packings were generated with a constant pressure tensor, where diagonal components are set to  $P_a = 10^{-4} \frac{k_B}{d}$  and off-diagonal components are set to zero, applied to an initially very dilute system; see Sec. II B for more details. The pressure damping for all components is  $P_{\text{damp}} = 2.25 \tau^{-1}$ . Figure 3 quantifies the impact of  $\mu_r$  and  $\mu_t$  on the coordination number without rattlers seen in Fig. 2 and predicted by constraint counting in Table I. The different panels in Fig. 3 isolate the impact of each friction mode. For sliding friction without rolling and twisting,  $Z$  decreases with increasing  $\mu_s$  as observed in previous volume-controlled packings [22]. As  $\mu_s \rightarrow 0$ ,  $Z$  approaches the 3D frictionless limit  $Z = 6$ . As  $\mu_s$  increases,  $Z$  continuously decreases to  $Z = 4$ , the limit predicted by constraint counting. Constraint counting predicts that  $Z$  decreases from six to four for any nonzero sliding friction. Shundyak *et al.* [19] found that, for 2D particles with sliding friction in the hard-sphere limit, the  $Z$  predicted from constraint counting equals the number of contacts minus the mobilized or plastic contacts per particle. Rolling and twisting friction modes have similar effects on  $Z$  with some distinctions.

The center two panels of Fig. 3 show that for low  $\mu_s$ ,  $Z$  is insensitive to rolling and twisting friction. The insensitivity

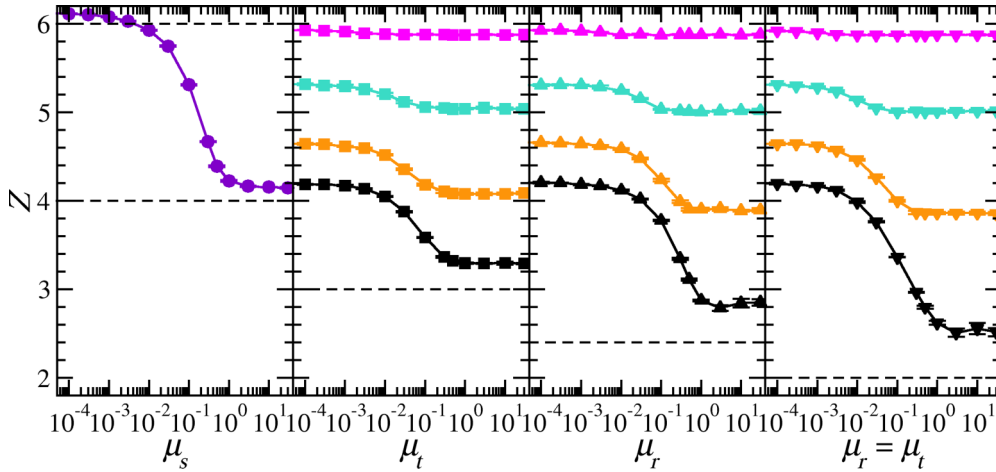


FIG. 3. Average coordination number without rattlers  $Z$  at jamming as a function of sliding ( $\mu_s$ , far left circles), twisting ( $\mu_t$ , for different  $\mu_s$  where  $\mu_r = 0$ , center left squares), rolling ( $\mu_r$ , for different  $\mu_s$  where  $\mu_t = 0$ , center right upward-facing triangles) frictions and where rolling and twisting frictions are set equal to each other (for different  $\mu_s$  where  $\mu_r = \mu_t$ , far right downward-facing triangles). The leftmost panel shows how  $Z$  behaves with  $\mu_r = \mu_t = 0.0$  (violet). For the other panels, data with different sliding frictions are drawn with the following distinct colors going from low to high:  $\mu_s = 0.01$ , (magenta), 0.1 (turquoise), 0.3 (orange), and 1 (black). Constraint counting values (horizontal black dashed lines) correspond with the cases shown in Table I. Packings are generated at  $P_a = 10^{-4} \frac{k_B}{d}$  with  $P_{\text{damp}} = 2.25 \tau^{-1}$ . Uncertainties are similar in size to the symbols, and solid lines are guides for the eye.

to  $\mu_r$  and  $\mu_t$  at low  $\mu_s$  is due to how friction is modeled. The contact point can move and disengage the rolling and twisting torques if the sliding friction is too low. As sliding friction is increased,  $\mu_s > 10^{-2}$ , rolling and twisting friction begin to affect  $Z$  in a similar way as sliding friction. Increasing sliding friction decreases  $Z$  at the low- $\mu_{r,t}$  values as well as increases the magnitude of the impact  $\mu_r$  and  $\mu_t$  have on  $Z$  at high- $\mu_{r,t}$  values. The scale of the decrease in  $Z$  depends on how many constraints a friction mode contributes. Because rolling friction contributes two constraints to rotational motion compared to one from twisting friction, rolling friction leads to a larger decrease in magnitude for  $Z$ . Constraint counting predicts those magnitudes; see Table I. Whereas with only sliding friction  $\lim_{\mu_s \rightarrow \infty} Z = 4$ , the inclusion of twisting friction leads to  $\lim_{\mu_{s,t} \rightarrow \infty} Z = 3.291 \pm 0.009$ , rolling friction leads to  $\lim_{\mu_{s,r} \rightarrow \infty} Z = 2.85 \pm 0.05$  and for all three frictions  $\lim_{\mu_{s,r,t} \rightarrow \infty} Z = 2.50 \pm 0.05$  (limiting  $Z$  values were taken as the minimum measured and reported in Fig. 3). Similar limiting behavior in  $Z$  was recently observed in shear jammed dense suspension simulations [3]. Any process that includes granular packings is likely impacted by the large decreases in the average number of contacts per particle from frictionless ( $Z = 6$ ) to large sliding, rolling, and twisting friction ( $Z = 2.5$ ).

These values are close to, but consistently greater than, the values predicted by constraint counting indicated by the dashed horizontal lines. A portion of the underestimation is because the  $Z$  reported in Fig. 3 is without rattlers. Taking rattlers out decreases the number of particles used to calculate  $Z$ , without much change in the number of contacts, and is not accounted for in constraint counting. To understand the larger constraint counting-simulation  $Z$  discrepancy, consider the  $Z = 2$  prediction for all three friction modes. Because there is no cohesion in this model, a particle with one contact is a rattler. Therefore, the only way for there to be a mechanically

stable system with  $Z = 2$  is if all nonrattlers have exactly two contacts. A stable packing of particles with only two contacts would be highly unlikely. The present system instead forms packings with a few  $Z > 2$  particles between chains of  $Z = 2$  for an average  $Z \geq 2.5$ . Previous simulations that included cohesion formed packings with  $Z = 2$  [50] support this explanation.

From the constraint counting predictions of the number of constraints per contact  $N_m^c$  and the critical value of mode  $m$  friction  $\mu_{m,c}$  at which  $Z$  is half way between the two limiting cases,  $Z_{m,c} = [Z(\mu_m \rightarrow 0) + Z(\mu_m \rightarrow \infty)]/2$ , the  $Z$  behavior can be approximated without simulation data as

$$Z = N^{\text{eqn}} - \tanh\left(\frac{\mu_s}{\mu_{s,c}}\right),$$

$$\times \left[ N_s^c + N_r^c \tanh\left(\frac{\mu_r}{\mu_{r,c}}\right) + N_t^c \tanh\left(\frac{\mu_t}{\mu_{t,c}}\right) \right], \quad (5)$$

where the number of equations  $N^{\text{eqn}}$  and constraints  $N_m^c$  are detailed in Table I. For this model,  $\mu_{s,c} \simeq \mu_{r,c} \simeq \mu_{t,c} \simeq 0.3$ , and thus  $Z = 6 - \tanh\left(\frac{\mu_s}{0.3}\right)[2 + 2 \tanh\left(\frac{\mu_r}{0.3}\right) + \tanh\left(\frac{\mu_t}{0.3}\right)]$ . The tanh function is chosen because it matches the correct limiting behavior and exponentially connects the limits. The sliding friction term,  $\tanh\left(\frac{\mu_s}{\mu_{s,c}}\right)$ , multiplies the rolling and twisting terms because no resistance to the sliding mode can lead granular particles to loose contact. The rolling and twisting modes of rotational motion cannot individually lead to contact disengagement. Because Eq. (5) is informed by constraint counting, its limits of  $Z$  are those predicted by constraint counting and do not match the simulation results. Equation (5) is a tool to estimate  $Z$  if the sliding, rolling, and twisting friction coefficients are known and could be used as an initial metric to select a material or model with desired packing properties.

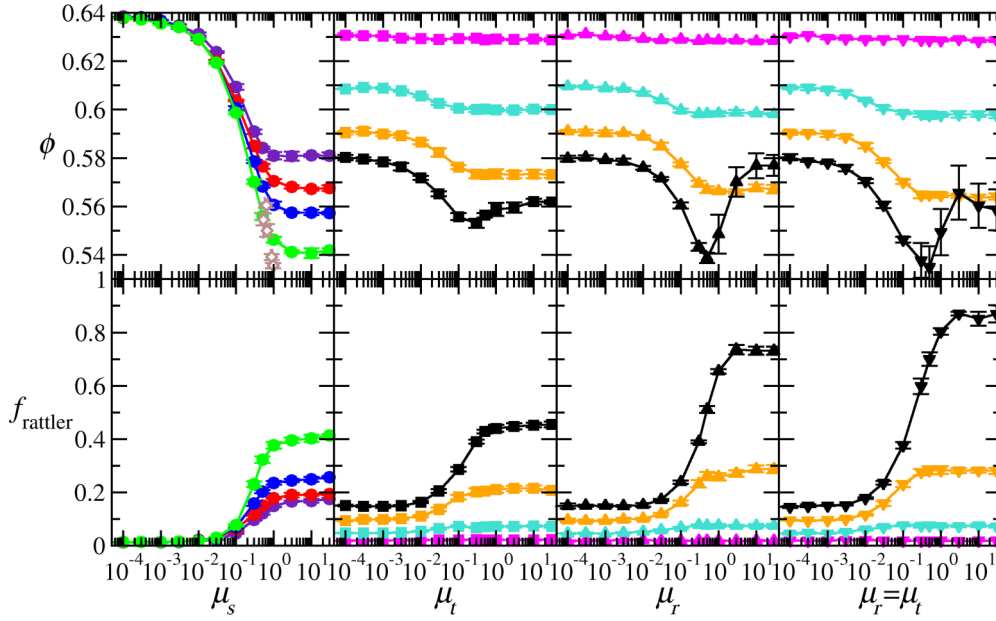


FIG. 4. Volume fraction ( $\phi$ , top) and fraction of rattlers ( $f_{\text{rattler}}$ , bottom) at jamming as a function of sliding ( $\mu_s$ , for different  $\mu_t = \mu_r$ , far left circles), twisting ( $\mu_t$ , for different  $\mu_s$  where  $\mu_r = 0$ , center left squares), rolling ( $\mu_r$ , for different  $\mu_s$  where  $\mu_t = 0$ , center right upward-facing triangles) frictions and where rolling and twisting friction coefficients are equal (for different  $\mu_s$  where  $\mu_r = \mu_t$ , far right downward-facing triangles). The leftmost panel shows a series of curves that represent different rolling and twisting friction coefficients:  $\mu_r = \mu_t = 0.0$  (violet),  $\mu_r = \mu_t = 0.01$  (red),  $\mu_r = \mu_t = 0.03$  (blue), and  $\mu_r = \mu_t = 0.1$  (green). For  $\mu_r, \mu_t > 0.1$ , there is little change in  $\phi(\mu_s)$  behavior. Experimental  $\phi$  values of Farrell *et al.* [29] for different materials with associated  $\mu_s$  are shown as brown diamonds. For the other panels, the colors are the same as Fig. 3.

The distribution of coordination numbers in high and low  $Z$  packings are visualized in Fig. 2. To be mechanically stable with so few contacts, a large fraction of the granular particles must be rattlers. Not only are there fewer nonrattler particles, but the distribution of nonrattlers is very heterogeneous. Figure 4 quantifies the fraction of rattlers as a function of the various friction modes. The rattler fraction increases monotonically with the friction coefficient of each mode.  $Z$  and  $f_{\text{rattler}}$  transitions from the low-friction to high-friction limits are similar. Rattlers become the majority with large friction  $\mu_{r,t}$  values if  $\mu_s > 0.3$ . Such microstructure must be very fragile (quantification of packing strength is subject of future study).

Figure 4 includes the volume fraction dependence on the different friction modes.  $Z$  and  $\phi$  behave similarly, except for a minimum in  $\phi$  for high  $\mu_s$ . The minimum in  $\phi$  is likely due to contacts saturating at the Coulomb friction criteria. Once constraining contacts saturate, the contacts can slide to form a denser packing, while maintaining their network. As seen with  $Z$  and  $f_{\text{rattler}}$ , sliding, rolling, and twisting friction cause a larger decrease in packing fraction.

The results shown in Figs. 2–4 are generated by applying a pressure  $P_a = 10^{-4} \frac{k_n}{d}$  to an initially dilute system. Figure 5 demonstrates that  $P_a = 10^{-4} \frac{k_n}{d}$  is within the low-pressure regime for frictionless, intermediate sliding friction and intermediate sliding, rolling, and twisting friction states. Decreasing the pressure by three orders of magnitude (from  $P_a = 10^{-4}$  to  $10^{-7} \frac{k_n}{d}$ ) changes the volume fraction by 0.004 or less for all friction states reported. The impact of increasing the friction coefficient or number of friction modes on volume

fraction and coordination number is considerably larger than the impact of decreasing the pressure below  $P_a = 10^{-4} \frac{k_n}{d}$ .

Figure 4 also shows the volume fraction of the packings generated by experiments. Experimental values are from Farrell *et al.* [29] and were performed by slowly settling spheres of different sliding friction coefficients, set by the material (steel, aluminum, acrylic, or teflon). The

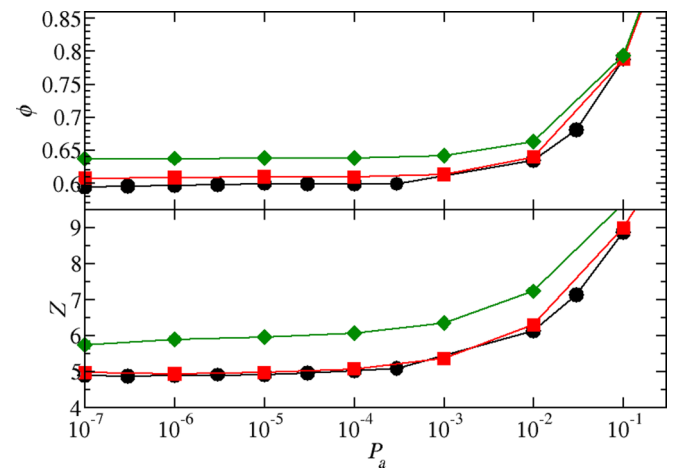


FIG. 5. Volume fraction ( $\phi$ , top) and coordination number ( $Z$ , bottom) at jamming as a function of the applied pressure for three different friction states:  $\mu_s = \mu_t = \mu_r = 0$  (green diamonds),  $\mu_s = 0.1, \mu_t = \mu_r = 0$  (red squares), and  $\mu_s = \mu_t = \mu_r = 0.1$  (black circles). Uncertainties are similar in size to the symbols, and solid lines are guides for the eye.

experimental  $\phi$  values are considerably below the simulation  $\phi$  values without rolling and twisting friction. As seen in Fig. 4, there is agreement with experiment for  $\phi$  only with rolling and twisting friction. To match experimental values for various acrylics, teflon, and steel,  $\mu_r = \mu_t = 0.1$  is required, while for aluminum our results for  $\mu_r = \mu_t = 0.03$  match the experiment. Those values required to match experiments are similar to the value of  $\mu_r = 0.07$  used in recent dense suspension simulations to match experimental shear viscosities [3]. Not only do rolling and twisting friction have a major impact on microstructure, as measured by  $Z$ , but they should be included in experimentally relevant particle models.

**IV. CONCLUSION**

Discrete-element, particle-based simulations of 3D granular particles demonstrated that rolling and twisting friction leads to large microstructural changes in mechanically stable packings, as insinuated by constraint counting. Agreement with experimental volume fractions was only attained with rolling and twisting friction ( $\mu_r = \mu_t = 0.1$ ) using this simulation protocol. These loose packings,  $\phi = 0.53$ , demonstrated the importance of different friction modes in real granular systems. The pressure-controlled compression protocol generated very loose packings with less computational effort than other methods. The barostat control parameters, including applied pressure, pressure damping, and drag, does impact the final packing properties, but these effects are small compared to the effect of friction. A deeper investigation into pressure-controlled simulation parameters and packing methods (compression, relaxation, and tapping) is the subject of a forthcoming article.

The decrease in the coordination number  $Z$  was predicted from constraint counting: both rolling and twisting friction impose extra constraints per contact. The decrease of the volume fraction and coordination number from low- to high-friction values was gradual for all three friction modes, as observed for sliding friction. Unlike sliding friction, the impact of resistance to rolling and twisting depended on the sliding resistance magnitude. When multiple friction modes were included, such as sliding with rolling or twisting, the coordination number predicted by constraint counting is considerably less than the value measured from simulations. Nonetheless, for very high friction,  $\mu_s = \mu_r = \mu_t = 1$ , a jammed system with  $Z = 2.5$  was observed. The majority of particles were rattlers in systems with such low coordination numbers, generally if  $Z < 3$ . Based on the knowledge gained from this information, an expression to predict  $Z(\mu_s, \mu_r, \mu_t)$  was proposed to aid constitutive models and future parametric studies.

The effect of rolling and twisting friction on packing illustrates the importance of including those modes to match experimental results and offers insight into the magnitude of those frictions required to induce property changes for other granular systems. Future work will focus on the impact of rolling and twisting friction on rheology and the material strength of packings. The publicly available rolling and twisting interaction models in LAMMPS enable the presented and future work.

**ACKNOWLEDGMENTS**

This work was performed, in part, at the Center for Integrated Nanotechnologies, an Office of Science User Facility operated for the U.S. Department of Energy (DOE) Office of Science. Sandia National Laboratories is a multi-mission laboratory managed and operated by National Technology and Engineering Solutions of Sandia, LLC., a wholly owned subsidiary of Honeywell International, Inc., for the U.S. DOE’s National Nuclear Security Administration under contract DE-NA-0003525. The views expressed in the article do not necessarily represent the views of the U.S. DOE or the United States Government.

**APPENDIX: ROLLING AND TWISTING PARAMETERIZATION**

Rolling and twisting resistance depend on the normal and tangential forces in most contact mechanics models [17]. Although simple, the spring-dashpot-slider system enables the study of each mode independently. This model allows for resistance to “pure” rolling. However, if there is no sliding friction, contacts can relax the rolling resistance by sliding off the contact [51–55].

Sources of twisting and sliding resistance are essentially the same—twisting friction is largely generated by rotational, versus translational, displacements within the contact area [17]. Therefore, twisting resistance should be related both to the tangential mode, from the sliding friction coefficient, and to the normal mode, from the contact area. There are more identified sources for rolling than twisting resistance. Microslip at the interface, inelastic deformation, and surface roughness all lead to resistance because of the pressure difference between the leading and trailing ends of the rolling contact [17]. Microslip, related to incipient sliding [17], occurs from creep of the interfacing material and the difference in shear forces at the interface when material in the contact area slips. Those phenomena arise from differences in material elastic constants, curvature, and torsion. The difference of strain on either side of the rolling contact causes inelastic deformation, another source of rolling resistance [38,56]. In most cases, inelastic deformation creates the largest rolling resistance contribution and can be characterized experimentally by a “hysteresis loss factor” [17]. Surface roughness and viscoelasticity can lead to rolling resistance, although likely at a lower magnitude than inelastic deformation and microslip. Surface roughness induces changes in the center-of-mass separation of the two bodies [57] and increases the real contact pressure [39]. Viscoelastic materials have a velocity-dependent rolling resistance, because of the balance in relaxation and observation times in rolling resistance for viscoelastic materials [58–60]. Approximations for the relative magnitude of rolling resistance have been made in the particle-based simulation literature.

Previous particle simulation studies that used spring interaction models made approximations for how the rolling spring constant  $k_r$  relates to more common parameters. Iwashita and Oda [10] set  $k_r = k_s/R^2$  by equating first-order approximations of the shear and rolling elastic displacement. Jiang *et al.* [61] instead assumed  $k_r = \frac{1}{12}k_n r_a^2$  and  $\gamma_r = \frac{1}{12}\gamma_n r_a^2$ ,

from Hertzian contact theory by representing a rolling contact as springs in parallel, where  $r_a$  is the contact radius and is calculated for each contact. A more exact analytical solution for a viscous sphere on a hard plane results in a relatively small value for  $k_r$  that is friction dependent and therefore does not work for our model [15]. Here we perform our own analysis of contact mechanics models to approximate the parameters of the twisting and rolling pseudoforces.

The twisting resistive moment in Hertzian theory is  $F_t = \frac{16}{3} G r_a^3 \theta_t$ , where  $\theta_t$  is the twisting angle,  $G$  is the shear modulus, and  $r_a$  is the contact radius [62]. This twisting model is associated with “no slip,” which yields a linear model with  $\theta_t$ . The contact radius can be estimated from the normal force as  $r_a = \left[ \frac{3F_n R(1-\nu^2)}{2E} \right]^{1/3}$ , where  $R$  is the particle radius,  $\nu$  is the Poisson ratio, and  $E$  is the elastic modulus [17]. By using the Hertzian approximation for  $r_a$  in the Lubkin twisting force  $F_t$  theory and by inserting  $k_t \theta_t$  and  $k_n \delta_t$  for tangential and normal Hookean-spring contact models, the following relationship for the twisting spring constant is found:  $k_t/k_n \propto \frac{8GR(1-\nu^2)}{E}$ . For steel  $G = 79.3$  GPa,  $E = 200$  GPa,  $\nu = 0.27$ , and therefore

$k_t/k_n \simeq 1.5$ . For rubber  $G = 0.0003$  GPa,  $E = 0.001$  GPa,  $\nu = 0.5$ , and therefore  $k_t/k_n \simeq 0.9$ . A similar analysis can also be carried out for the rolling pseudoforce. Based on Johnson’s formulation of elastic deformation [63,64], the moment due to elastic creep between spheres is  $\mathbf{F}_r = \frac{32(2-\nu)}{9(3-2\nu)} G r_a^3 \nu_r$ . Using the same assumption for the contact radius of two elastic bodies used for twisting, we get  $\mathbf{F}_r = \frac{16(2-\nu)(1-\nu^2)}{3(3-2\nu)} \frac{G}{E} R \mathbf{F}_n \theta_r$ . Since we model  $F_r = k_r \theta_r$  and  $F_n = k_n \delta_n$ , the ratio of rolling and normal forces scales as  $k_r/k_n \propto \frac{16(2-\nu)(1-\nu^2)}{3(3-2\nu)} \frac{G}{E} R$ , for elastic deformation. For steel  $k_r/k_n \simeq 0.7$ , and for rubber  $k_r/k_n \simeq 0.5$ .

To empirically identify realistic parameters for the rolling and twisting modes, DEM simulations of simple configurations were performed. Two overlapping suspended spheres, with fixed translational positions (and fixed  $\mathbf{F}_n$ ), were given an initial relative rolling or twisting angular velocity. Nonphysical values of  $k_m$  and  $\gamma_m$  gave long-lived oscillations and/or overdamped decay of the torque. The rolling spring-dashpot slider has realistic behavior for  $0 < k_r/\gamma_r < 1$ , yet  $k_r/\gamma_r > 1$  is realistic if  $k_n/k_r < 10$ . Realistic twisting angle and torque behavior was found for  $0 < k_t/\gamma_t \leq 2$ .

- 
- [1] A. E. Skinner, A note on influence of interparticle friction on shearing strength of a random assembly of spherical particles, *Geotechnique* **19**, 150 (1969).
- [2] P. Mort, J. N. Michaels, R. P. Behringer, C. S. Campbell, L. Kondic, M. Kheiripour Langroudi, M. Shattuck, J. Tang, G. I. Tardos, and C. Wassgren, Dense granular flow—A collaborative study, *Powder Technol.* **284**, 571 (2015).
- [3] A. Singh, C. Ness, R. Seto, J. J. de Pablo, and H. M. Jaeger, Shear Thickening and Jamming of Dense Suspensions: The Roll of Friction, *Phys. Rev. Lett.* **124**, 248005 (2020).
- [4] N. Estrada, A. Taboada, and F. Radjai, Shear strength and force transmission in granular media with rolling resistance, *Phys. Rev. E* **78**, 021301 (2008).
- [5] Y. Liu, H. Liu, and H. Mao, The influence of rolling resistance on the stress-dilatancy and fabric anisotropy of granular materials, *Granular Matter* **20**, 12 (2018).
- [6] W. Wu, G. Ma, W. Zhou, D. Wang, and X. Chang, Force transmission and anisotropic characteristics of sheared granular materials with rolling resistance, *Granular Matter* **21**, 88 (2019).
- [7] R. Mari and R. Seto, Force transmission and the order parameter of shear thickening, *Soft Matter* **15**, 6650 (2019).
- [8] B. M. Guy, J. A. Richards, D. J. M. Hodgson, E. Blanco, and W. C. K. Poon, Constraint-Based Approach to Granular Dispersion Rheology, *Phys. Rev. Lett.* **121**, 128001 (2018).
- [9] J. P. Bardet, Observations on the effects of particle rotations on the failure of idealized granular materials, *Mech. Mater.* **18**, 159 (1994).
- [10] K. Iwashita and M. Oda, Rolling resistance at contacts in simulation of shear band development by DEM, *J. Eng. Mech.* **124**, 285 (1998).
- [11] A. Tordesillas, J. Peters, and M. Muthuswamy, Role of particle rotations and rolling resistance in a semi-infinite particulate solid indented by a rigid flat punch, *ANZIAM J.* **46**, C260 (2005).
- [12] Y. Wang and P. Mora, Modeling wing crack extension: Implications for the ingredients of discrete element model, in *Earthquakes: Simulations, Sources and Tsunamis*, edited by K. Tiampo, D. Weatherley, and S. Weinstein (Birkhäuser, Basel, 2008), pp. 609–620.
- [13] O. Reynolds, On rolling-friction, *Phil. Trans. R. Soc.* **166**, 155 (1875).
- [14] H. Hertz, On the contact of elastic solids, *J. Reine Angew. Math.* **92**, 156 (1882).
- [15] N. V. Brilliantov and T. Pöschel, Rolling friction of a viscous sphere on a hard plane, *Europhys. Lett.* **42**, 511 (1998).
- [16] T. Pöschel, T. Schwager, and N. V. Brilliantov, Rolling friction of a hard cylinder on a viscous plane, *Eur. Phys. J. B* **10**, 169 (1999).
- [17] K. L. Johnson, *Contact Mechanics* (Cambridge University Press, Cambridge, 1985).
- [18] L. E. Silbert, D. Ertas, G. S. Grest, T. C. Halsey, and D. Levine, Geometry of frictionless and frictional sphere packings, *Phys. Rev. E* **65**, 031304 (2002).
- [19] K. Shundyak, M. van Hecke, and W. van Saarloos, Force mobilization and generalized isostaticity in jammed packings of frictional grains, *Phys. Rev. E* **75**, 010301(R) (2007).
- [20] E. Somfai, M. van Hecke, W. G. Ellenbroek, K. Shundyak, and W. van Saarloos, Critical and noncritical jamming of frictional grains, *Phys. Rev. E* **75**, 020301(R) (2007).
- [21] C. Song, P. Wang, and H. A. Makse, A phase diagram for jammed matter, *Nature (London)* **453**, 629 (2008).
- [22] L. E. Silbert, Jamming of frictional spheres and random loose packing, *Soft Matter* **6**, 2918 (2010).
- [23] S. Torquato, T. M. Truskett, and P. G. Debenedetti, Is Random Close Packing of Spheres Well Defined?, *Phys. Rev. Lett.* **84**, 2064 (2000).
- [24] G. D. Scott and D. M. Kilgour, The density of random close packing of spheres, *J. Phy. D Appl. Phys.* **2**, 863 (1969).



- [25] R. L. Brown and P. G. W. Hawksley, Effect of container walls on packing density of particles, *Nature (London)* **157**, 585 (1946).
- [26] G. D. Scott, Packing of spheres: Packing of equal spheres, *Nature (London)* **188**, 908 (1960).
- [27] R. Rutgers, Packing of spheres, *Nature (London)* **193**, 465 (1962).
- [28] M. Jerkins, M. Schröter, H. L. Swinney, T. J. Senden, M. Saadatfar, and T. Aste, Onset of Mechanical Stability in Random Packings of Frictional Spheres, *Phys. Rev. Lett.* **101**, 018301 (2008).
- [29] G. R. Farrell, K. M. Martini, and N. Menon, Loose packings of frictional spheres, *Soft Matter* **6**, 2925 (2010).
- [30] S. Dagois-Bohy, B. P. Tighe, J. Simon, S. Henkes, and M. van Hecke, Soft-Sphere Packings at Finite Pressure but Unstable to Shear, *Phys. Rev. Lett.* **109**, 095703 (2012).
- [31] K. C. Smith, I. Srivastava, T. S. Fisher, and M. Alam, Variable-cell method for stress-controlled jamming of athermal, frictionless grains, *Phys. Rev. E* **89**, 042203 (2014).
- [32] I. Srivastava and T. S. Fisher, Slow creep in soft granular packings, *Soft Matter* **13**, 3411 (2017).
- [33] P. A. Cundall and O. D. L. Strack, A discrete numerical model for granular assemblies, *Geotechnique* **29**, 47 (1979).
- [34] S. Luding, Cohesive, frictional powders: Contact models for tension, *Granular Matter* **10**, 235 (2008).
- [35] J. S. Marshall, Discrete-element modeling of particulate aerosol flows, *J. Comput. Phys.* **228**, 1541 (2009).
- [36] S. F. Foerster, M. Y. Louge, H. Chang, and K. Allia, Measurements of the collision properties of small spheres, *Phys. Fluids* **6**, 1108 (1994).
- [37] To use this interaction model in LAMMPS [41], use the following commands: `pair_style granular` followed by `pair_coeff * * hooke  $k_n$   $\gamma_n$  damping mass_velocity tangential linear_history  $k_s$   $\gamma_s/\gamma_n$   $\mu_s$  rolling sds  $k_r$   $\gamma_r$   $\mu_r$  twisting sds  $k_t$   $\gamma_t$   $\mu_t$ . See LAMMPS documentation at lammps.sandia.gov for more details.`
- [38] D. Tabor, The mechanism of rolling friction. II. The elastic range, *Proc. R. Soc. Lond. A* **229**, 198 (1955).
- [39] J. Halling, Effect of deformation of the surface texture on rolling resistance, *Br. J. Appl. Phys.* **10**, 172 (1959).
- [40] G. Carbone and C. Putignano, A novel methodology to predict sliding and rolling friction of viscoelastic materials: Theory and experiments, *J. Mech. Phys. Solids* **61**, 1822 (2013).
- [41] S. Plimpton, Fast parallel algorithms for short-range molecular dynamics, *J. Comput. Phys.* **117**, 1 (1995).
- [42] W. Shinoda, M. Shiga, and M. Mikami, Rapid estimation of elastic constants by molecular dynamics simulation under constant stress, *Phys. Rev. B* **69**, 134103 (2004).
- [43] G. J. Martyna, D. J. Tobias, and M. L. Klein, Constant pressure molecular dynamics algorithms, *J. Chem. Phys.* **101**, 4177 (1994).
- [44] M. Parrinello and A. Rahman, Polymorphic transitions in single crystals: A new molecular dynamics method, *J. Appl. Phys.* **52**, 7182 (1981).
- [45] D. J. Durian, Foam Mechanics at the Bubble Scale, *Phys. Rev. Lett.* **75**, 4780 (1995).
- [46] T. G. Mason, M.-D. Lacasse, G. S. Grest, D. Levine, J. Bibette, and D. A. Weitz, Osmotic pressure and viscoelastic shear moduli of concentrated emulsions, *Phys. Rev. E* **56**, 3150 (1997).
- [47] C. S. O'Hern, L. E. Silbert, A. J. Liu, and S. R. Nagel, Jamming at zero temperature and zero applied stress: The epitome of disorder, *Phys. Rev. E* **68**, 011306 (2003).
- [48] To apply this symmetric pressure tensors in LAMMPS [41], use `fix 1 all nph/sphere x  $P_a$   $P_a$   $P_{damp}$  y  $P_a$   $P_a$   $P_{damp}$  z  $P_a$   $P_a$   $P_{damp}$  xy 0.0 0.0  $P_{damp}$  yz 0.0 0.0  $P_{damp}$  xz 0.0 0.0  $P_{damp}$  nreset 1 pchain 0. See LAMMPS documentation at lammps.sandia.gov for more details.`
- [49] J. C. Maxwell, On the calculation of the equilibrium and stiffness of frames, *Philos. Mag.* **27**, 294 (1865).
- [50] W. Liu, Y. Jin, S. Chen, H. A. Makse, and S. Li, Equation of state for random sphere packings with arbitrary adhesion and friction, *Soft Matter* **13**, 421 (2017).
- [51] K. M. Khan and G. Bushell, Comment on "Rolling friction in the dynamic simulation of sandpile formation," *Physica A* **352**, 522 (2005).
- [52] M. J. Jiang, H. S. Yu, and D. Harris, Bond rolling resistance and its effect on yielding of bonded granulates by DEM analyses, *Int. J. Numer. Anal. Meth. Geomech.* **30**, 723 (2006).
- [53] H. P. Zhu and A. B. Yu, A theoretical analysis of the force models in discrete element method, *Powder Technol.* **161**, 122 (2006).
- [54] J. Ai, J. F. Chen, J. M. Rotter, and J. Y. Ooi, Assessment of rolling resistance models in discrete element simulations, *Powder Technol.* **206**, 269 (2011).
- [55] Y. Wang, F. Alonso-Marroquin, and W. W. Guo, Rolling and sliding in 3-D discrete element models, *Particuology* **23**, 49 (2015).
- [56] K. R. Eldredge and D. Tabor, The mechanism of rolling friction. I. The plastic range, *Proc. R. Soc. Lond. A* **229**, 181 (1955).
- [57] R. C. Drutowski, Energy losses of balls rolling on plates, *J. Basic Eng.* **81**, 233 (1959).
- [58] W. D. May, E. L. Morris, and D. Atack, Rolling friction of a hard cylinder over a viscoelastic material, *J. Appl. Phys.* **30**, 1713 (1959).
- [59] D. G. Flom and A. M. Bueche, Theory of rolling friction for spheres, *J. Appl. Phys.* **30**, 1725 (1959).
- [60] S. C. Hunter, The Hertz problem for a rigid spherical indenter and a viscoelastic half-space, *J. Mech. Phys. Solids* **8**, 219 (1960).
- [61] M. J. Jiang, H. S. Yu, and D. Harris, A novel discrete model for granular material incorporating rolling resistance, *Comput. Geol.* **32**, 340 (2005).
- [62] J. L. Lubkin, The torsion of elastic spheres in contact, *ASME Trans. J. App. Mech.* **18**, 183 (1951).
- [63] K. L. Johnson, The effect of spin upon the rolling motion of an elastic sphere on a plane, *Trans. ASME, J. Appl. Mech.* **25**, 332 (1958).
- [64] K. L. Johnson, The effect of a tangential contact force upon the rolling motion of an elastic sphere on a plane, *Trans. ASME, J. Appl. Mech.* **25**, 339 (1958).